

## NONLINEAR DECENTRALIZED POSITION CONTROL OF ELECTROHYDRAULIC ACTUATORS IN ROAD SIMULATION

**Beshahwired Ayalew**

The Pennsylvania State University  
The Pennsylvania Transportation Institute  
201 Transportation Research Building  
University Park, PA 16802  
Email: beshah@psu.edu  
Phone:(814)863-8057  
Fax:(814)865-3039

**Bohdan T. Kulakowski**

The Pennsylvania State University  
The Pennsylvania Transportation Institute  
201 Transportation Research Building  
University Park, PA 16802  
Email: btk1@psu.edu  
Phone:(814)865-1893  
Fax:(814)865-3039

### ABSTRACT

In this paper, a nonlinear position tracking controller is derived based on feedback linearization to globally linearize the nonlinear dynamics of an electrohydraulic actuator with nonlinear state feedback. A detailed computer model is developed for a four-post road simulation system with a transit bus as the test vehicle. Using this model, comparisons are conducted between the proposed nonlinear decentralized controller and a traditional linear decentralized controller. Previously introduced interaction measures suitable for time domain analysis of nonlinear systems confirm that, for the test vehicle considered, load plate position loop interactions are quickly eliminated by either the linear or nonlinear decentralized position controllers. The performance of the road simulator as gauged by a position tracking error metric for a typical rough road profile is improved by over 60% across all actuators and response matching of sprung mass vertical acceleration PSD is likewise improved by over 50% when using the nonlinear decentralized controller.

**Keywords:** road simulator, four-poster, electrohydraulic actuators, input-output linearization, decentralized control, actuator interaction, feedback linearization

### INTRODUCTION

Road simulators enable the in-laboratory evaluation of vehicle structural durability and vehicle dynamics for ride comfort and Noise and Vibration Harshness (NVH) without having to run the vehicle's drive train on an actual road surface. They can also be used in the assessment of pavement damage and the study of road-vehicle interaction.

In a typical tire-coupled four-post road simulator (four-poster), electrohydraulic actuators are employed to apply vertical excitations through the tires of the test vehicle. Fig 1 shows a schematic of the main components for one leg of a four-poster. The test vehicle's wheels are mounted on the wheel or load plates located at one end of a double acting piston. A servovalve modulates flow to and from the top and bottom piston-actuator cylinder chambers.

The individual actuators are usually controlled using linear decentralized PID load-plate position controllers, which

sometimes include differential pressure ( $\Delta p$ ) feedback for improved damping [1]. Here, by decentralized control we mean the control of each actuator independently of the others, in an essentially SISO (Single Input Single Output) setup.

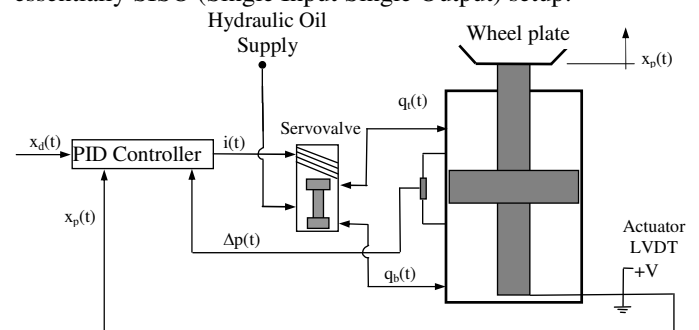


**Figure 1 Schematic of one leg of a four-poster**

However, conventional PID ( $+\Delta p$ ) control loops acting on electrohydraulic hardware have practical difficulties such as stability margins, actuator and test fixture bandwidth limitations and inevitable nonlinearities in the electrohydraulic system. Furthermore, when considering all four actuators and the test vehicle, the whole system is a dynamically coupled nonlinear system. These all have a negative bearing on the effort to match the drive signals ( $x_d(t)$ ) with the actual piston position in a repeatable manner using only PID ( $+\Delta p$ ) control loops. The testing community employing electrohydraulic actuators has found it necessary to use the PID controller as an 'inner' control loop and include 'outer' compensation loops to improve control accuracy, stability and repeatability [1, 2]

A summary of the 'outer'-loop compensation techniques, which generally involve iterative (mainly off-line) computation of drive signals  $x_d(t)$  that attempt to match field measured responses with on-simulator responses, is given in [1-4]. These approaches generally apply the iterations with Multiple Input Multiple Output (MIMO) setups to systematically address the issue of nonlinearity and load cross-coupling. The 'inner'-loop is generally left to the decentralized PID ( $+\Delta p$ ) loops.

In this paper, we investigate the potential of a decentralized nonlinear position controller, which is derived based on input-output (IO) or partial feedback linearization [5, 6] to improve the performance of the decentralized 'inner'-control loops of a road simulator. Perhaps the earliest study on the application of feedback linearization to electrohydraulic actuators was that of Axelson and Kumar [7] in 1988. Their work presented the derivation of the control law emphasizing the nonlinearity of valve flow only. Hahn, et al [8] derived a more detailed controller for the position tracking case and presented limited results from simulations with an inertia load. Vossoughi and Donath[9] presented an analysis and derivation of feedback linearizing controller for a velocity tracking robotic application. Del Re and Isidori [10] discussed the application of feedback linearization by using linear-bilinear model approximations of a nonlinear hydrostatic transmission. In this paper, we present a study of decentralized Near IO linearizing control of electrohydraulic actuators in four-post road simulation.

The rest of the paper is organized as follows. First, we present the nonlinear electrohydraulic actuator model and nonlinear full-bus model of a transit bus used in this study. We then derive the nonlinear controller to be implemented in the road simulator system model. We shall then briefly look at interactions between the decentralized position controls loops, and follow this by a comparative study of road simulator performance under the nonlinear and PID+ $\Delta p$  decentralized controllers. Finally, we present the conclusions of the paper.

## NOMENCLATURE

$A_b, A_t$	piston areas for the bottom and top chambers, respectively
$b_{lf}, b_{rf}, b_{lr}, b_{rr}$	distances from each unsprung mass c.g. to the left and right tires as shown in Fig.3
$C_L$	leakage coefficient
$C_{ti}; i=1,2,3,4$	tire damping coefficients
$C_{v,i}; i=1,2,3,4$	valve coefficient referred to each port
$d_{lf}, d_{rf}, d_{lr}, d_{rr}$	distances from the sprung mass c.g. to each suspension attachment point in Fig.3
$e$	position tracking error
$f_{di}, i=1,2,3,4$	nonlinear function for shock absorber damping
$F_f$	friction force on piston
$F_L$	load force on piston
$f_p$	nonlinear feedback term given by Eq (15)
$F_p$	fluid pressure force on piston
$f_{si}, i=1,2,3,4$	interpolation function for air suspension stiffness
$F_{si}, i=1,2,3,4$	suspension forces
$F_{ti}, i=1,2,3,4$	tire forces
$g$	acceleration due to gravity
$g_p$	nonlinear feedback term given by Eq (16)
$G_V$	static gain of the valve
$i, j, k$	indexing integers
$I_p$	Pitch moment of inertia for sprung mass
$I_r, I_{uf}, I_{ur}$	roll moments of inertia for sprung and front and rear unsprung masses, respectively

$i_v$	servovalve current
$i_{voff}$	offset current to account for abrasion wear and lap
$\bar{i}_v$	net servovalve current
$k_1, k_2, k_3$	control gains in Eq (19)
$K_p, K_b, K_D,$ $K_{\Delta p}$	PID+ $\Delta p$ controller gains in Eq (21)
$K_{ti}; i=1,2,3,4$	tire stiffness
$K_{v,i}; i=1,2,3,4$	valve coefficients defined with spool position
$l_f, l_r$	distance from sprung mass c.g. to each axle, in Fig. 3
$m_p$	lumped mass of piston, load plate and oil
$M_s$	mass of sprung mass
$M_{uf}, M_{ur}$	mass of unsprung mass, front and rear respectively
$p_b, p_t$	pressure in the bottom and top cylinder chambers, respectively
$p_R$	return pressure at servovalve
$p_S$	supply pressure at servovalve
$q_b, q_t$	flow to the bottom and from the top cylinder chambers, respectively
$q_{e,b}, q_{e,t}$	external leakage from the bottom and top chambers, respectively
$q_i$	internal leakage in cylinder
$s$	Laplace variable
$t, T, t_o$	time, smoothing factor, and step time, respectively, used in Eq (28)
$v$	intermediate control defined by Eq (19)
$V_b, V_t$	bottom and top cylinder chamber volumes, respectively
$v_p$	piston velocity
$X_d$	amplitude of reference magnitude in Eq (28)
$x_p$	piston position
$x_d$	desired or reference position trajectory
$x_v$	servovalve spool position
$x_{voff}$	offset servovalve spool position to account for abrasion wear and lap
$\bar{x}_v$	net servovalve spool position
$z_s, z_{uf}, z_{ur}$	vertical position of c.g. of sprung mass, and front and rear unsprung mass, respectively
$z_{ui}, z_{si}$ $i=1,2,3,4$	positions of tire and suspension attachment points, respectively, w.r.t. zero roll and pitch
$\beta_e$	effective bulk modulus
$\theta$	pitch angle of sprung mass
$\Delta p$	differential pressure ( $\Delta p = p_b - p_t$ )
$\phi, \phi_{uf}, \phi_{ur}$	roll of body, and front and rear unsprung mass roll, respectively

## MODEL DEVELOPMENT

### Electrohydraulic Actuator Model

Models of electrohydraulic actuators are quite widely available in the literature [11-14]. The model presented here applies to a four-way critically centered servovalve close-

coupled with a double-ended translational piston actuator as shown in Fig. 2. In the figure,  $q_t$  and  $q_b$ , are flow rate from the top chamber and to the bottom chamber of the cylinder, respectively.  $q_i$  represents internal leakage flow between the two chambers and  $q_{e,t}$  and  $q_{e,b}$  are external leakage from the top and bottom chambers, respectively.  $A_t$  and  $A_b$  represent the effective piston areas of the top and bottom piston face, respectively, and  $V_t$  and  $V_b$  designate the volumes of oil in the top and bottom chambers, respectively, corresponding to the center position ( $x_p=0$ ) of the piston. These volumes also include the respective volumes of oil in the short pipelines between the close-coupled servovalve and actuator.

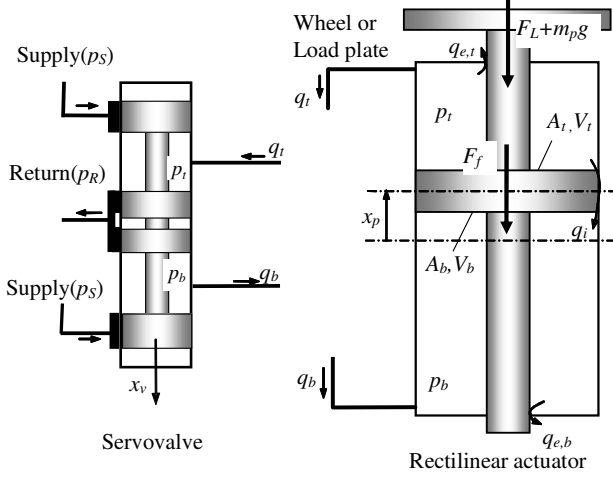


**Figure 2 Schematic of actuator and servovalve**

It shall be assumed here that the pressure dynamics in the lines between the servovalve and the actuator are negligible due to the close-coupling. Even for a long-stroke actuator in a flight simulator application, where close-coupling may not be feasible, Van Schothorst [13] showed that the pressure dynamics in the actuator chambers need not be modeled using distributed parameter models and that they can be assumed uniform in each chamber. Starting with the continuity equation and the state equation with the effective oil bulk modulus for the cylinder chambers, it can be shown that the chamber pressure dynamics are given by (see, for example [14]):

$$\frac{dp_b}{dt} = \frac{\beta_e}{V_b + A_b x_p} (q_b - A_b \dot{x}_p + q_i - q_{e,b}) \quad (1)$$

$$\frac{dp_t}{dt} = \frac{\beta_e}{V_t - A_t x_p} (-q_t + A_t \dot{x}_p - q_i - q_{e,t}) \quad (2)$$

These equations show that the hydraulic capacitance, and hence the pressure evolution in the two chambers depends on the piston position, thereby introducing nonlinearity in the chamber pressure dynamics. The external leakage flows,  $q_{e,b}$ , and  $q_{e,t}$ , are negligible. The internal leakage past the piston seals is usually assumed to be laminar, with a leakage coefficient,  $C_L$ , as follows:

$$q_i = C_L (p_t - p_b) \quad (3)$$

The predominantly turbulent flows through the sharp-edged control orifices of a spool valve to and from the two sides of the cylinder chambers are modeled by nonlinear expressions as follows [12, 14, 15]:

$$q_b = K_{v,1} s g(x_v) \operatorname{sgn}(p_s - p_b) \sqrt{|p_s - p_b|} - K_{v,2} s g(-x_v) \operatorname{sgn}(p_b - p_R) \sqrt{|p_b - p_R|} \quad (4)$$

$$q_t = K_{v,3} s g(x_v) \operatorname{sgn}(p_t - p_R) \sqrt{|p_t - p_R|} - K_{v,4} s g(-x_v) \operatorname{sgn}(p_s - p_t) \sqrt{|p_s - p_t|} \quad (5)$$

where the function,  $s g(x)$ , is defined by:

$$s g(x) = \begin{cases} x, & x \geq 0 \\ 0, & x < 0 \end{cases} \quad (6)$$

Here,  $K_{v,i}$ ,  $i = 1, 2, 3, 4$  are the valve coefficients whose estimation shall be described shortly.

The state equations governing piston motion are derived considering the actuator loading model. The force on the actuator piston due to the oil pressure is given by:

$$F_p = A_b p_b - A_t p_t \quad (7)$$

Denoting the friction force on the piston by  $F_f$  and the load force, which is the tire force in the present case, by  $F_L$ , and applying Newton's Second Law, we have:

$$\dot{x}_p = v_p \quad (8)$$

$$\dot{v}_p = \frac{1}{m_p} [A_b p_b - A_t p_t - F_L - F_f - m_p g] \quad (9)$$

Equations (1), (2), (8) and (9), with  $q_b$  and  $q_t$  given by Eqs (4) and (5), constitute the state space model for the servovalve and loaded actuator subsystem. These equations also contain the major nonlinearities in the system, which are the variable hydraulic capacitance and the square root flow rate versus pressure drop relations. Further nonlinearity is introduced in Eq (9) by a nonlinear friction force, which could include Coulomb, static, and viscous components [3], a nonlinear load force  $F_L$  which also transmits nonlinear suspension forces.

## CONTROLLER DERIVATION

### Basic Assumptions

For the control law derivation, the servovalve is considered to be critically centered, i.e., underlap/overlap lengths are neglected. Instead, an offset value of the valve position can be estimated during calibration to take into account any abrasion-induced null offsets [14]. Also, the valve spool dynamics are neglected. This implies that the valve spool position is assumed to be related to the servovalve current with a static gain  $G_v$ , as:

$$\bar{i}_v = G_v \bar{x}_v \quad (10)$$

where,  $\bar{i}_v = i_v - i_{v,off}$ , and  $\bar{x}_v = x_v - x_{v,off}$ , with  $i_{v,off}$  and  $x_{v,off}$  representing the current offset and valve spool position offset, respectively. In this paper, we choose to consider the servovalve current as the control variable. The flow rates to and from the cylinder chambers are then rewritten as follows:

$$q_b = C_{v,1} s g(\bar{i}_v) \operatorname{sign}(p_s - p_b) \sqrt{|p_s - p_b|} - C_{v,2} s g(-\bar{i}_v) \operatorname{sign}(p_b - p_R) \sqrt{|p_b - p_R|} \quad (11)$$

$$q_t = C_{v,3}sg(\bar{i}_v)sign(p_t - p_R)\sqrt{|p_t - p_R|} - C_{v,4}sg(-\bar{i}_v)sign(p_S - p_t)\sqrt{|p_S - p_t|} \quad (12)$$

where the new valve coefficients referenced to the current are given by:

$$C_{v,i} = G_v K_{v,i} \quad i = 1, 2, 3, 4 \quad (13)$$

The form of the flow rate equations given by Eqs (11) and (12) allow us to estimate the valve coefficients  $C_{v,i}$  from quick offline experiments; see for example ref [15] (pp 184-186).

We also assume that accumulators are close-coupled on the servovalve manifold on the return and supply lines. We can then justifiably assume constant values for the supply and return pressures at the servovalve [16].

To simplify the analysis, we assume perfect knowledge of the necessary parameters for the nonlinear controller. Robust control versions are described in [3]. Aside from the determination of parametric and measurement uncertainty bounds, there should be no major difficulty in switching to the robust versions. We also assume that the four actuators are identical in terms of modeling parameters. However, their decentralized controllers can be tuned separately.

### Load Plate Position Tracking Controllers

The first and second derivatives of the output position,  $x_p$ , as given by Eqs (8) and (9) do not contain the control input,  $\bar{i}_v$ . However, further differentiation of Eq (9) gives:

$$\ddot{x}_p = f_p(x_p, \dot{x}_p, p_b, p_t, \dot{F}_f, \dot{F}_L) + g_p(x_p, p_b, p_t, \text{sgn}(\bar{i}_v))\bar{i}_v \quad (14)$$

where the nonlinear functions,  $f_p$  and  $g_p$ , are respectively:

$$f_p(x_p, \dot{x}_p, p_b, p_t) = \frac{1}{m_p} (-\dot{x}_p \beta_e \left( \frac{A_b^2}{V_b + A_b x_p} + \frac{A_t^2}{V_t - A_t x_p} \right) + \frac{A_b \beta_e C_L (p_t - p_b)}{V_b + A_b x_p} + \frac{A_t \beta_e C_L (p_t - p_b)}{V_t - A_t x_p} - \dot{F}_f - \dot{F}_L) \quad (15)$$

$$g_p(x_p, p_b, p_t, \text{sgn}(\bar{i}_v)) = \begin{cases} \frac{1}{m_p} \left( \frac{A_b \beta_e C_v}{V_b + A_b x_p} \text{sgn}(p_S - p_b) \sqrt{|p_S - p_b|} + \frac{A_t \beta_e C_v}{V_t - A_t x_p} \text{sgn}(p_t - p_R) \sqrt{|p_t - p_R|} \right) & \text{for } \bar{i}_v \geq 0 \\ \frac{1}{m_p} \left( \frac{A_b \beta_e C_v}{V_b + A_b x_p} \text{sgn}(p_b - p_R) \sqrt{|p_b - p_R|} + \frac{A_t \beta_e C_v}{V_t - A_t x_p} \text{sgn}(p_S - p_t) \sqrt{|p_S - p_t|} \right) & \text{for } \bar{i}_v < 0 \end{cases} \quad (16)$$

Equation (14), with the nonlinear functions  $f_p$  and  $g_p$  defined by Eqs (15) and (16), respectively, contains all the major modeled nonlinearities from fluid compliance and turbulent orifice flow as well as friction and load forces. From Eq (14), piecewise input-output (IO) linearization [5, 6] can be performed in the respective domains ( $\bar{i}_v \geq 0$  and  $\bar{i}_v < 0$ ) and the nonlinearities can be cancelled by choosing the control law:

$$\bar{i}_v = \frac{1}{g_p(x_p, p_b, p_t, \text{sgn}(\bar{i}_v))} (\ddot{v} - f_p(x_p, \dot{x}_p, p_b, p_t, \dot{F}_f, \dot{F}_L)) \quad (17)$$

The closed loop position dynamics reduces to the triple integrator:

$$\ddot{x}_p = v \quad (18)$$

which can easily be stabilized by state feedback. It also gives an exponentially convergent tracking (provided the internal dynamics are stable) when the new dummy input  $v$  is chosen as:

$$v = \ddot{x}_d - k_3(\ddot{x}_p - \ddot{x}_d) - k_2(\dot{x}_p - \dot{x}_d) - k_1(x_p - x_d) \quad (19)$$

where  $x_d$  is the desired position profile. It can easily be shown that there are no internal dynamics for position tracking [3]. Combining Eqs (18) and (19), the dynamics of the closed loop tracking error,  $e = x_p - x_d$ , reduce to:

$$\ddot{e} + k_3\dot{e} + k_2e + k_1e = 0 \quad (20)$$

The gains  $k_1$ ,  $k_2$ , and  $k_3$  can be chosen to place the poles of the closed loop tracking error dynamics strictly in the left half s-plane. This could be done by using direct pole placement or posing the problem as a linear optimal control problem [3]. Direct pole placement involves deciding on the location of the three poles for the closed loop error dynamics given by Eq.(20) and invoking pole placement routines to compute the three gains  $k_1$ ,  $k_2$ , and  $k_3$ . This latter approach is used in this paper.

It is important to note that the nonlinear control expression Eq (17) cannot be solved "as is", since it contains the control variable,  $\bar{i}_v$ , on both sides of an equation involving the *signum* (*sgn*) function. In practice, during the digital implementation, the sign of the value of  $\bar{i}_v$  at the previous time step can be used to compute the value of  $\bar{i}_v$  at the current time step, supposing that the current does not change signs at a rate faster than the base sampling rate. However, it is difficult to analytically prove that this approach does not lead to control chatter. This chatter problem has not been previously reported in the literature that discusses feedback linearization for hydraulic drives [8-10]. In addition, we have not experienced this problem in any of our experiments with force and position control on an experimental electrohydraulic actuator [3]. Nevertheless, the name Near input-output (Near IO) linearization is adopted in this paper to make the explicit distinction that the present controller is not a true IO linearizing controller in the traditional sense, but it is very close.

For the purpose of comparison, we consider the traditional linear PID+ $\Delta p$  controller, which is given by:

$$\dot{i}_v = K_P e + K_I \int e dt + K_D \dot{e} + K_{\Delta p} \Delta p \quad (21)$$

where  $\Delta p$  is the differential pressure ( $p_p - p_t$ ).

### Full-Bus Model

We consider a full-bus model of a transit bus with dependent suspensions as shown in Fig.3. The parameters of the model are extracted from various sources [17-20]. The air suspensions and shock absorbers are modeled as nonlinear elements. Yaw motions of the bus are considered irrelevant on the four-poster. Pitch and roll motions of the body (sprung mass) and of the unsprung masses are assumed to be small enough to allow use of small angle approximations for the pitch and roll motions. The resulting model has seven degrees of freedom comprising of the following: bounce of the rear and

front unsprung masses ( $z_{ur}$ ,  $z_{uf}$ ), roll motion of the rear and front unsprung masses ( $\phi_{ur}$ ,  $\phi_{uf}$ ), and the pitch ( $\theta$ ), roll ( $\phi$ ) and bounce ( $z_s$ ) motions of the sprung mass.

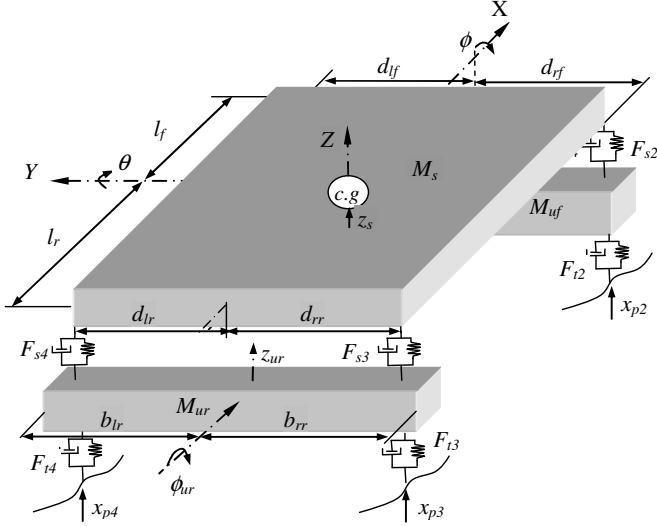


**Figure 3 Model of full-bus with dependent suspensions**

The equations of motion for the front and rear unsprung masses ( $M_{uf}$ ,  $M_{ur}$ ) and the sprung mass ( $M_s$ ) are:

$$\begin{aligned}
 M_{uf} \ddot{z}_{uf} &= \sum_{i=1,2} (F_{ti} + F_{si}) - M_{uf} g \\
 I_{uf} \ddot{\phi}_{uf} &= b_{lf} (F_{t1} + F_{s1}) - b_{rf} (F_{t2} + F_{s2}) - T_{arf} \\
 M_{ur} \ddot{z}_{ur} &= \sum_{i=3,4} (F_{ti} + F_{si}) - M_{ur} g \\
 I_{ur} \ddot{\phi}_{ur} &= b_{lr} (F_{t4} + F_{s4}) - b_{rr} (F_{t3} + F_{s3}) - T_{arr} \\
 M_s \ddot{z}_s &= -\sum_{i=1}^4 F_{si} - M_s g \\
 I_p \ddot{\theta} &= \sum_{i=1,2} l_f F_{si} - \sum_{i=3,4} l_r F_{si} - T_{ap} \\
 I_r \ddot{\phi} &= -d_{lf} F_{s1} - d_{lr} F_{s4} + d_{rf} F_{s2} + d_{rr} F_{s3} + T_{arf} + T_{arr}
 \end{aligned} \quad (22)$$

Note that in the above equations, we have assumed compressive tire forces to be positive to easily replace the load force  $F_L$  in the actuator model described above. These tire forces,  $F_{ti}$ , are approximated by:

$$F_{ti} = K_{ti} (x_{pi} - z_{ui}) + C_{ti} (\dot{x}_{pi} - \dot{z}_{ui}) \quad i = 1, 2, 3, 4 \quad (23)$$

And the nonlinear suspension and damping forces,  $F_{si}$ , are given by:

$$F_{si} = f_{si} (z_{si} - z_{ui}) + f_{di} (\dot{z}_{si} - \dot{z}_{ui}) \quad i = 1, 2, 3, 4 \quad (24)$$

where,  $f_{si}$  and  $f_{di}$  represent interpolations in tables of air suspension stiffness data and shock absorber damping data, respectively. The displacements of the suspension attachment points,  $z_{si}$ ,  $i=1, 2, 3, 4$ , are given by:

$$\begin{aligned}
 z_{s1} &= z_s - l_f \theta + d_{lf} \phi \\
 z_{s2} &= z_s - l_f \theta - d_{rf} \phi \\
 z_{s3} &= z_s + l_r \theta - d_{rr} \phi \\
 z_{s4} &= z_s + l_r \theta + d_{lr} \phi
 \end{aligned} \quad (25)$$

The displacements of the wheel centers,  $z_{ui}$ ,  $i=1, 2, 3, 4$ , are given by:

$$\begin{aligned}
 z_{u1} &= z_{uf} + b_{lf} \phi_{uf} \\
 z_{u2} &= z_{uf} - b_{rf} \phi_{uf} \\
 z_{u3} &= z_{ur} - b_{rr} \phi_{ur} \\
 z_{u4} &= z_{ur} + b_{lr} \phi_{ur}
 \end{aligned} \quad (26)$$

Not shown in Fig.3 are the auxiliary roll stiffness and damping torques ( $T_{arr}$ ,  $T_{arf}$ ) and the body pitch stiffness and damping torque ( $T_p$ ). These are included to account for any additional stiffness and damping provided by the mounting conditions and elements of the suspension geometry such as torsion bars and radius rods. The defining equations are:

$$\begin{aligned}
 T_{arr} &= K_{arr} (\phi_{ur} - \phi) + C_{arr} (\dot{\phi}_{ur} - \dot{\phi}) \\
 T_{arf} &= K_{arf} (\phi_{uf} - \phi) + C_{arf} (\dot{\phi}_{uf} - \dot{\phi}) \\
 T_{ap} &= K_{ap} \theta + C_{ap} \dot{\theta}
 \end{aligned} \quad (27)$$

where,  $K_{arr}$ ,  $K_{arf}$ ,  $K_{ap}$  are the respective auxiliary torsional stiffnesses, and  $C_{arr}$ ,  $C_{arf}$  and  $C_{ap}$  are the auxiliary torsional damping coefficients.

## SIMULATION STUDY

### Road Simulator System Model

Note that, for the full-bus model, the piston positions,  $x_{pi}$ , of the four actuators represent road profile inputs to the test vehicle as a subsystem. On the other hand, the tire forces,  $F_{ti}$ ,  $i=1, 2, 3, 4$ , can be considered as the outputs of the full-bus model and as the load forces on the actuator load-plates.

Figure 4 shows the input-output interconnection of the road simulator as a system. For simplicity, the figure shows the interconnection of a quarter-bus to the electrohydraulic actuator model including its corresponding decentralized controller. The case of the full-bus model has a similar structure.

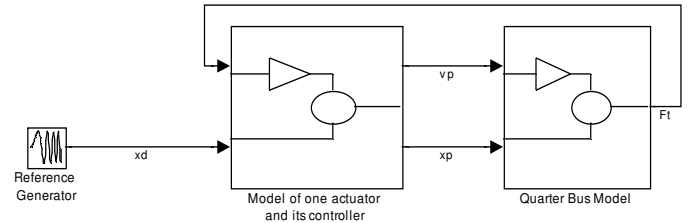


**Figure 4 Road Simulator System Model**

### Tuning the Decentralized Controllers

It was first attempted to tune the decentralized controllers of the four actuators using a nonlinear quarter-bus model with parameters corresponding to the full-bus model. The equations describing a quarter-bus can easily be derived from Eq (22) by ignoring all pitch and roll motions and focusing on one corner of the bus. Two different quarter-bus models were employed to

tune the controllers of the front and rear actuators, since the loading on the front portion of the bus differs from the rear.

However, the best actuator control gains determined using the quarter-bus model led to instability when used on the coupled four-actuator case of the full-bus model. The problem was particularly severe when tuning the  $K_p$ -gains of the PID+ $\Delta p$  controllers. This is to be expected because the quarter-bus model ignores motion cross-coupling that is relevant in the more realistic full-bus model. The gains are, therefore, re-tuned interactively by considering the useable gains on the full-bus four-actuator system as well. The problem of instability with higher gains or faster pole locations is much less acute for the Near IO linearizing controller. This is because the Near IO linearizing controller uses some of the cross-coupling information via feedback of the tire forces.

Figure 5 shows a basic comparison between the tracking performance of the Near IO linearizing controller and a PID+ $\Delta p$  controller for one of the rear actuators loaded with a quarter-bus, employing gains that were useable in the four-actuator full-bus case as well. To generate a smooth step reference, the tangent hyperbolic function was used:

$$x_d = X_d \tanh\left(\frac{t-t_o}{T}\right) \quad (28)$$

Parameters  $t_o$  and  $X_d$  determine the instant and magnitude of the step, while  $T$  is a smoothing parameter. As  $T \rightarrow 0$ , this function approaches the Heaviside step function with sharp corners. For the data in Fig.5,  $T=0.05$ , and for the PID+ $\Delta p$  controller,  $K_p$ -gain=3mA/cm,  $K_{\Delta p}$ -gain=0.001mA/MPa,  $K_D=K_I=0$ . All three poles of the Near IO linearizing controller were placed at  $s=-400$  for a response that doesn't saturate the control current ( $\pm 9$ mA) for the chosen step reference.

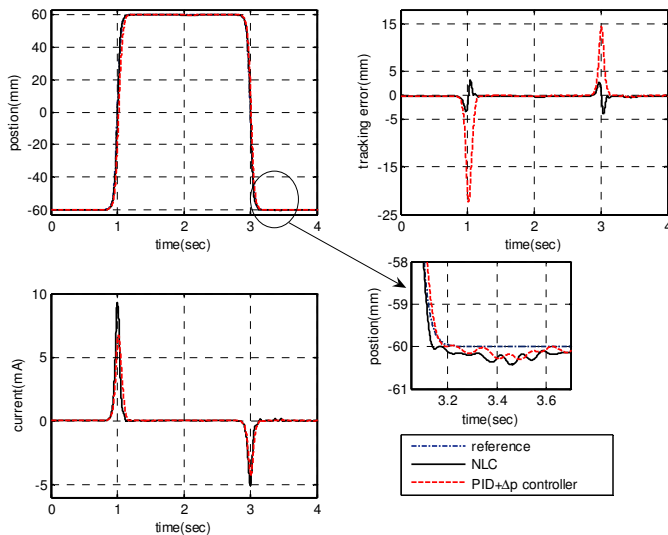


**Figure 5 Tuning the Near IO linearizing controller (NLC) and a PID+ $\Delta p$  controller using a quarter-bus model**

A similar comparison was obtained for the front actuators. With the lighter mass and softer suspension associated with the front portion of the bus, the closed-loop poles for the Near IO linearizing controller could be pushed further to the left (to  $s=-650$ ) than it was possible with the rear actuators without saturating the control current or inducing instability of the four-actuator, full-bus system. The  $K_p$ -gain of the PID+ $\Delta p$  controller

could likewise be increased further (to 18mA/cm) without destabilizing the full-bus case. However, the comparative performance of the Near IO linearizing controller with the PID+ $\Delta p$  controller remains similar to that shown in Fig. 5. It is remarked, here, that the decentralized Near IO linearizing controller shows consistently less tracking error peak magnitudes than the decentralized PID+ $\Delta p$  controller.

### Interaction in Decentralized Piston Position Control Loops

The effect of interaction due to dynamic load cross-coupling on the decentralized control of each of the four-poster's actuator load-plate positions is briefly investigated in this section. To this end, the nonlinear system is first brought to a steady-state and then, one by one, the reference input (desired position) for one actuator position control loop is step changed while the references to the other actuators are kept zero.

Figure 6 shows one set of responses following a step change in the reference input for the rear left actuator controller from 0 to 80 mm (with  $T=0.05$ ) while zero reference is given to the controllers of the other actuators.

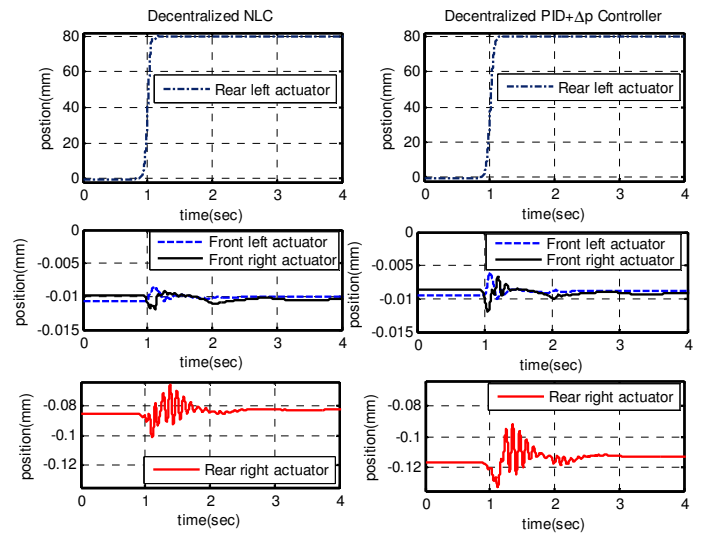


**Figure 6 Actuator interaction in terms of load-plate positions with decentralized Near IO linearizing control (NLC) (left column) and PID+ $\Delta p$  control (right column)**

It can be seen from Fig.6 that, following the step disturbance, clearly, interaction is present between the decentralized control loops, but the degree of interaction is very small with either controller. The strongest interaction is side to side. That is, the rear left actuator interacts the most with the rear right actuator, and so on. Furthermore, the advantage of the Near IO linearizing controller over the PID+ $\Delta p$  controller does not appear to be significant in terms of minimizing interactions for the test vehicle considered.

The Relative Gain Array (*RGA*) is often used to assess interactions between decentralized control loops [21-24]. The time domain *RGA*, first suggested by [24], and used in [22, 25] is given by:

$$RGA(t) = \hat{g}(t) .* [\hat{g}(t)]^T \quad (29)$$

where the product ( $.*$ ) is an element by element multiplication and  $\hat{g}(t)$  is a matrix given by (for 2x2 case):

$$\hat{g}(t) = \begin{bmatrix} \left( \frac{\delta y_1}{\delta u_1} \right)_{u_2} & \left( \frac{\delta y_1}{\delta u_2} \right)_{u_1} \\ \left( \frac{\delta y_2}{\delta u_1} \right)_{u_2} & \left( \frac{\delta y_2}{\delta u_2} \right)_{u_1} \end{bmatrix} \quad (30)$$

where the  $\delta y_i$  are computed as integral deviations (from steady state(ss) values preceding the step disturbances) by

$$\delta y_i = \int (y_i - y_{iss}) d\tau \quad i = 1, 2, 3, 4 \quad (31)$$

The smooth step changes  $\delta u_i$  are computed in a similar manner. Note that the  $RGA(t)$  is a matrix of the same size  $\hat{g}(t)$ , which is 4x4 for the four-poster, and that, it is invariant under scaling. The closer an element  $\lambda_{i,j}$  of the  $RGA(t)$  is to 1, the stronger is the coupling between that particular input ( $x_{dj}$ ) and output ( $x_{pi}$ ). Therefore, the closer the  $RGA$  is to the identity matrix, the stronger the diagonal dominance of the system. The  $RGA$  number is also used as a measure of this closeness of the  $RGA$  to the identity matrix. It is computed by:

$$RGA \text{ number}(t) = \|RGA(t) - I\|_{sum} \quad (32)$$

The above remarks imply that when the  $RGA$  is close to the identity matrix, or equivalently when the  $RGA$  number is close to zero, a decentralized control loop employing a diagonal input-output pairing of  $x_{di}$  with  $x_{pi}$  suffers minimal interaction effects from other loops. Here  $i$  and  $j$  are indexes 1, 2, 3, 4 corresponding to the front left, front right, rear right and rear left actuator, respectively. Figure 7 shows the diagonal  $RGA$  elements and the  $RGA$  number computed by repeating the tests shown in Fig. 6 with all actuators.

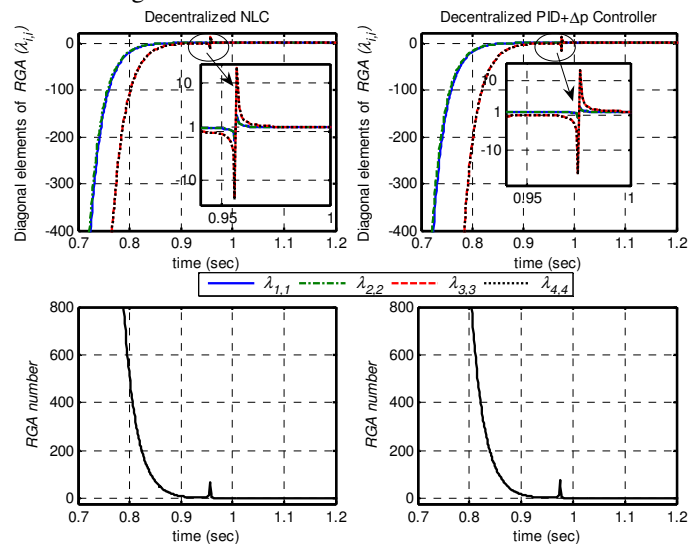


**Figure 7** Diagonal elements of the  $RGA$  and the  $RGA$  number with decentralized Near IO linearizing control (NLC) (left column) and PID+ $\Delta p$  control (right column).

Note that the time scales shown in Fig.7 are within the rise-time of the step change in the reference. The large initial magnitudes of the diagonal  $RGA$  elements show that interactions are present in the system, but they die away very

quickly. The diagonal  $RGA$  elements rapidly approach one and the  $RGA$  number vanishes to zero very fast, showing the diagonal dominance of the decentralized position control loops. Furthermore, the  $RGA$  number with the Near IO linearizing controller dies away somewhat faster than the PID+ $\Delta p$  controller, but overall the two controllers perform similarly in suppressing interactions.

The switch in the sign of the diagonal  $RGA$  elements magnified in the inserts in Fig.7 is typical of systems showing inverse response [24]. Figure 6 shows that inverse response is evident in the actuators on the right side (both front and rear), when positive step reference is applied to the rear left actuator. As Witcher and McAvoy [24] pointed out, these large and switching  $RGA$  magnitudes are normally expected to cause control difficulty. In the present application, however, the interactions die away very fast, even faster than the ‘smooth’ step change (considered reasonable for this application), showing the effectiveness of the present decentralized feedback controllers (either linear or nonlinear).

In the paper [25], we used short time-span open-loop tests, without any control on all actuators, to trace the physical cause of this behavior. When one actuator moves in response to current input, cross-coupling in the vehicle’s dynamics causes load changes on the other actuators even if they were operating with a closed valve (zero current). However, the actuators do not move much, or any induced motion due to these load changes dies away quickly, similar to the closed-loop case shown in Fig.6. This can certainly be attributed to the good stiffness property of the electrohydraulic actuator.

We conclude this section by stating that the four-poster with decentralized control of actuator load-plate positions and the transit bus as a test vehicle behaves as an almost diagonal MIMO system. Any interactions exhibited are quickly suppressed by either the linear or nonlinear decentralized control.

### Performance of the Road Simulator under Decentralized Position Control

In this section, we include comparisons of the tracking performance of the two decentralized controllers using a typical road profile as the desired load-plate position trajectory ( $x_{di}$ ).

Recall from the model interconnection described previously that on the road simulator, the vehicle model can be considered to be driven by the actuator load-plate positions ( $x_{pi}$ ) as inputs. Here, we shall also consider the case where the full-bus model is driven directly by the actual road profile (replacing  $x_{pi}$  by the road profile,  $x_{di}$ ). We shall refer to vehicle response obtained under the latter case as the ‘on-the-road’ response. The performance of the road simulator system in replicating road excitation shall be evaluated by comparing on-simulator response to ‘on-the-road’ response.

Road profiles typically contain such a widely varying excitation that it would be inconvenient to investigate the effectiveness of the road simulator by scrutinizing time responses or power spectral density (PSD) plots. We therefore use some performance metrics that give single numbers which quantitatively indicate the quality of the road simulation.

A simple metric is the  $rms$  value of a response parameter  $X$ , which is given by:

$$X_{RMS} = \sqrt{\frac{\sum_{i=1}^N X_i^2}{N}} \quad (33)$$

where  $N$  is the number of data points considered. We shall compare the *rms* values of the sprung and unsprung mass acceleration responses on the road simulator and “on-the-road”. Brauer [26] suggested the related metric called Euclidean error. It is computed by taking the *rms* value of the difference between two discrete signals  $X$  and  $Y$  of length  $N$  as follows:

$$Eucl = \sqrt{\frac{\sum_{i=1}^N (X_i - Y_i)^2}{N}} \quad (34)$$

Since vehicle responses are often described in the frequency domain, we shall also compute the Power Spectral Density (PSD) for the sprung mass vertical acceleration for both on-simulator and “on-the-road” responses.

The International Roughness Index (IRI) is often used to characterize roughness of road surfaces [27]. The typical road profile we consider in this section is of IRI 170 (in/mile), which falls under a mediocre road classification. The road profile data used here have been taken from ref [27] and they are actual road profiles from field measurements for a total distance of 500 meters. The profiles differentiate between left-side and right-side tracks and are available as tables of horizontal travel vs. vertical deviation. This data are easily converted to time signals for an assumed vehicle speed. We consider speeds of 35 mph (56 km/hr) and 55 mph (88 km/hr) in this section. Note also that the time lag (= *wheel base/vehicle speed*) differentiates the reference profiles applied to the front and rear actuators.

Recall that for a nonlinear system, the performance of the controller (particularly of the Near IO linearizing one) depends on the reference trajectory. Therefore, the two decentralized controllers were re-tuned for the specific road profile considered here. Since the time waveform corresponding to a road profile depends on the vehicle speed, one may consider tuning the controller gains for each vehicle speed as well. However, for the basic comparison presented in this section, this was not found necessary. The three-closed-loop pole locations for the front actuator Near IO linearizing controllers were set at  $s=-1000$  and those of the rear ones were set at  $s=-900$ ; for the front actuator PID+ $\Delta p$  controllers, P-gain= 18 mA/cm and  $\Delta p$ -gain=0.004 mA/MPa and for the rear ones, P-gain= 3.5 mA/cm and  $\Delta p$ -gain=0.005 mA/MPa. These gains were determined for a well-tuned tracking performance with the vehicle speed at 35mph and were used for 55 mph as well.

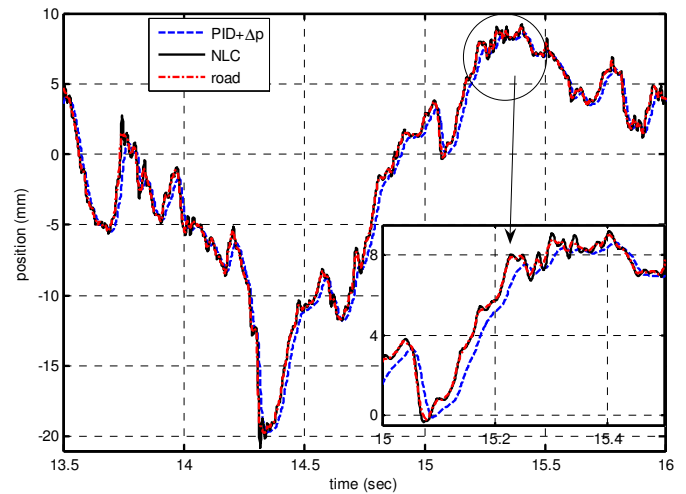


**Figure 8 Rear left actuator load-plate position for a section of an IRI 170 road at 55 mph with the Near IO linearizing position tracking controller (NLC) and the PID+ $\Delta p$  controller.**

Figure 8 shows a section of the time waveform plots for the load-plate tracking behavior for the rear left actuator. Note that the Near IO linearizing controller gives an almost perfect tracking compared to the PID+ $\Delta p$  controller. Table 1 summarizes the tracking performance for all actuators covering the whole 500 m-long profile using the Euclidean position error metric. The position error is computed as the instantaneous error between the actuator position output and the road-profile reference for the particular actuator, considering time lags and left-side/right-side track differences. As should be expected, for both controllers (which were tuned at 35 mph), the Euclidean error is higher at 55 mph, but in all cases, the Near IO linearizing controller outperforms the PID+ $\Delta p$  controller in terms of matching each load-plate position with the respective desired road profile. The improvement in the tracking performance with the Near IO linearizing controller is more than about 60% at all actuators and at both vehicle speeds.

**Table 1 Comparison of the tracking performance for the two decentralized controllers**

Vehicle speed (km/hr (mph))	Decentralized controller	Euclidean position error (mm)			
		Front Left	Front Right	Rear Right	Rear Left
56(35)	PID+ $\Delta p$	0.166	0.189	0.645	0.640
	NLC	0.060	0.072	0.088	0.072
88(55)	PID+ $\Delta p$	0.338	0.362	0.897	0.893
	NLC	0.137	0.162	0.211	0.177

Table 2 shows a further comparison in terms of vehicle response parameters, namely, the *rms* values of sprung and unsprung mass accelerations for the whole 500 m-long profile. The on-simulator responses using the decentralized Near IO linearizing controller have better matching with the “on-the-road” responses than those using the PID+ $\Delta p$  controller. We

also note the improvement with the Near IO linearizing controller is reduced when looking at vehicle responses instead of actuator load-plate tracking errors. This can be attributed to the filtering characteristics of the tire and the suspension.

**Table 2 Comparison of *rms* values of on-simulator and “on-the-road” responses**

Vehicle speed (km/hr (mph))	Response parameter (accelerations (g))	Form of excitation (actuator control or direct road profile input)		
		PID+ $\Delta p$	NLC	road
56(35)	sprung mass	0.0116	0.0120	0.0119
	front unsprung mass	0.3242	0.3201	0.3176
	rear unsprung mass	0.3926	0.4564	0.4377
88(55)	sprung mass	0.0172	0.0187	0.0184
	front unsprung mass	0.5400	0.0538	0.5205
	rear unsprung mass	0.6089	0.7022	0.6700

Finally, we look at a comparison of responses in the frequency domain. Figure 9 shows the power spectral density (PSD) of the on-simulator and “on-the-road” sprung mass acceleration responses with the vehicle speed at 55 mph. For lower frequencies, there is little difference between the two decentralized controllers. However, at higher frequencies, the on-simulator response with the Near IO linearizing controller matches the “on-the-road” response much better than the on-simulator response with the PID+ $\Delta p$  controller.

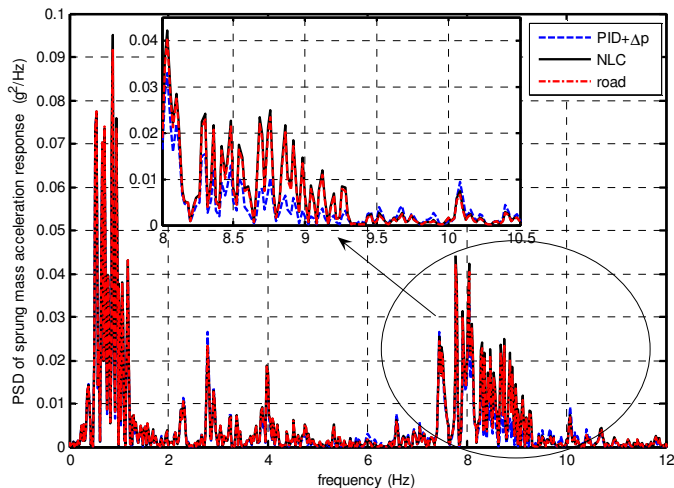


**Figure 9 PSD of Sprung mass acceleration in the frequency domain for an IRI 170 road at 55mph with the decentralized Near IO linearizing position controller (NLC) and the decentralized PID+ $\Delta p$  controller**

Table 3 summarizes the differences between the PSDs of the on-simulator and “on-the-road” sprung mass acceleration responses for the whole 500 m-long profile at vehicle speeds of 35 and 55 mph. For this table, the Euclidean error is computed as the *rms* error between the on-simulator response and “on-

the-road” response at each discrete frequency point of the FFT (Fast Fourier Transform). For both controllers, it can be seen that the Euclidean PSD error is higher at 55 mph than at 35 mph (as should be expected, since tuning was done for 35 mph), but in all cases, the Near IO linearizing controller (NLC) keeps the error metric smaller than the PID+ $\Delta p$  controller by over 50%.

**Table 3 Comparison of the Euclidean error in the sprung mass acceleration PSD**

Vehicle speed (km/hr (mph))	Decentralized controller	Euclidean PSD error in sprung mass acceleration ((g <sup>2</sup> /Hz)x10 <sup>-6</sup> )
56 (35)	PID+ $\Delta p$	8.3967
	NLC	4.0320
88 (55)	PID+ $\Delta p$	16.7080
	NLC	4.5079

## CONCLUSIONS

In this paper, the decentralized control of the electrohydraulic actuators of a four-post road simulation system has been considered. A nonlinear controller that cancels the nonlinearities in the electrohydraulic actuator has been derived. A full-bus model of a transit bus, employing nonlinear air-suspensions and nonlinear shock-absorbers, has been adopted as the test vehicle model.

Using simulations of the road simulator as a system, it has been shown that in terms of eliminating interaction, decentralized control of actuator load-plate positions is very effective for the test vehicle considered. This implies that for the actuator to follow road profile measurements, the decentralized control of the actuators’ load-plate positions provides a satisfactory solution. It is also highlighted that this arose naturally from the good stiffness property of electrohydraulic actuators. Furthermore, in terms of suppressing interactions, the advantage for the Near IO linearizing controller over the PID+ $\Delta p$  controller appears to be small. The tracking performance of the individual loops, however, is improved significantly with the Near IO linearizing controller.

Using *rms* performance metrics, the performance of the road simulation system for tracking an actual road profile of mediocre roughness is investigated. It has been shown that the Near IO linearizing controller outperforms the PID+ $\Delta p$  controller in all the cases considered. In particular, there is more than a 60% improvement in matching load-plate positions with reference profiles with the nonlinear controller. It is noted that there is a corresponding improvement in terms of response matching as well. For example, there is a more than 50% reduction in the Euclidean error of matching PSDs of the sprung mass vertical acceleration when using the Near IO linearizing controller compared to the PID+ $\Delta p$  controller.

Recall that practical road simulation approaches generally consider the road simulation system (including the actuators and the test vehicle) as a MIMO unit, with the decentralized position controllers as an ‘inner’-loops to the ‘outer’-loop iterative drive signal generators that attempt to match on-simulator responses to desired (on road) responses. The fact

that significantly better tracking of actuator load plate positions are obtained with the decentralized Near IO linearizing controller has important implications for these response-replication road simulation approaches. It improves the linearity and speed of response of the 'inner'-loop, so that iterative drive signal generation converges faster and 'outer'-loop MIMO compensators work better.

## REFERENCES

1. Soderling, S., Sharp, M., and Leser, C., 1999, "Servo-Controller Compensation Methods: Selection of the Correct Techniques for Test Applications," in VIII International Mobility Technology Conference and Exhibit, SAE, 1999-01-3000, Sao Paulo, Brazil, Oct 4-6.
2. De Cuyper, Joris, Verhaegen, Michel, and Swevers, Jan, 2003, "Off-Line Feed-Forward and  $H_\infty$  Feedback Control on a Vibration Rig," *Control Engineering Practice*, Vol. 11, pp. 129-140.
3. Ayalew, Beshahwired, 2005, "Nonlinear Control of Multi-Actuator Electrohydraulic Systems Based on Feedback Linearization with Application to Road Simulation," Ph D Dissertation, in Mechanical Engineering, The Pennsylvania State University.
4. de Pont, J., 1993, "Rating Heavy Vehicle Suspensions for 'road friendliness'," *Heavy Vehicle Systems, Special Series, Int. J. of Vehicle Design*, Vol. 1(1), pp. 20-33.
5. Slotine, Jean-Jacques E., and Li, Wieping, 1991, *Applied Nonlinear Control*. Prentice Hall.
6. Khalil, Hassan K., 2002, *Nonlinear Systems*, Third ed., Prentice Hall.
7. Axelson, Steve, and Kumar, K. S. P., 1988, "Dynamic Feedback Linearization of a Hydraulic Valve-Actuator Combination," in the 1988 American Control Conference, Atlanta, Georgia, June 15-17, 1988.
8. Hahn, H., Piepenbrink, A., and Leimbach, K.-D., 1994, "Input/Output Linearization Control of an Electro Servo-Hydraulic Actuator," in the Third IEEE Conference on Control Applications, pp. 995-1000, Glasgow, UK.
9. Vossoughi, Gholamreza and Donath, Max, 1995, "Dynamic Feedback Linearization for Electrohydraulically Actuated Control Systems," *Journal of Dynamic Systems, Measurement, and Control*, Vol. 117, pp. 468-477, December 1995.
10. Del Re, Luigi, and Isidori, Alberto, 1995, "Performance Enhancement of Nonlinear Drives by Feedback Linearization of Linear-Bilinear Cascade Models," *IEEE Transactions on Controls Systems Technology*, Vol. 3(3), pp. 299-308, September 1995.
11. Dransfield, Peter, 1981, *Hydraulic Control Systems: Design and Analysis of their Dynamics*. Springer-Verlag.
12. Merritt, Herbert E., 1967, *Hydraulic Control Systems*. John Wiley and Sons, New York.
13. Van Schothorst, Gerard, 1997, "Modelling of Long-Stroke Hydraulic Servo-Systems for Flight Simulator Motion Control and System Design," PhD Thesis, Delft University of Technology, the Netherlands.
14. Kugi, Andreas, 2001, *Non-linear Control Based on Physical Models*. Springer, London.
15. Jelali, Mohieddine, and Kroll, Andreas, 2003, *Hydraulic Servo-Systems: Modelling, Identification and Control*. - (Advances in Industrial Control). Springer-Verlag, London.
16. Ayalew, Beshahwired, and Kulakowski, Bohdan T., 2005, "Modeling Supply and Return Line Dynamics for an Electrohydraulic Actuation System," *ISA Transactions*, Vol. 44(2), April 2005.
17. Genta, Giancarlo, 1997, *Motor Vehicle Dynamics: Modeling and Simulation*. World Scientific Publishing Co., River Edge, New Jersey.
18. Nova Bus Inc., Transit Bus Division, 2002, "Low Floor Bus Dimensions and Air Suspension Specifications," David Klinikowski.
19. Xiao, Jie, 2002, "System Identificatin for Transit Buses Using a Hybrid Genetic Algorithm," PhD Thesis, in Mechanical Engineering, The Pennsylvania State University, University Park.
20. Zhang, J., Xinglong, Y., Yi, L., Wangyu, W., Lingzhang, M., Yu, F., and Lin, W., 2002, "Performance Simulation Research on Bus with Air Suspension," 2002-01-3093, SAE.
21. Bristol, Edgar H., 1966, "On a New Measure of Interaction for Multivariable Process Control," *IEEE Transactions on Automatic Control*, Vol. 11(1), pp. 133-134, January 1966.
22. Ramachandran, S. and Dransfield, P., 1993, "Interaction between the Actuators in Loaded Multi-Channel Electrohydraulic Drives," *Transactions of ASME, Journal of Dynamic Systems, Measurement and Control*, Vol. 115, pp. 291-302, June 1993.
23. Skogestad, Sigurd and Postelthwaite, Ian, 1996, *Multivariable Feedback Control*. John Wiley & Sons, Chichester, United Kingdom.
24. Witcher, M.F., and McAvoy, T.J., 1977, "Interacting Control Systems: Steady State and Dynamic Measurement of Interaction," *ISA Transactions*, Vol. 16(3), pp. 35-41.
25. Ayalew, Beshahwired and Kulakowski, Bohdan T., 2005, "Decentralized Control of Interacting Electrohydraulic Actuators in Road Simulation," *Int. Journal of Heavy Vehicle Systems*, Vol. 13(4).
26. Brauer, Matthew, 2000, "Control Algorithms for a Road Simulator in Durability Testing of Transit Buses," Masters Thesis, The Pennsylvania State University, University Park, May 2000.
27. UMTRI, 2005, "International Roughness Index (IRI)," Universtiy of Michigan Transportation Research Institute, <http://www.umtri.umich.edu/erd/roughness/index.html>